Supplementary Information for
Post-stroke reorganization of transient brain activity characterizes deficits and recovery of cognitive functions

Elvira Pirondini[1,2,3,4,12], Nawal Kinany[1,2,5,12], Cécile Le Sueur[2], Joseph C. Griffis[6], Gordon L. Shulman[6], Maurizio Corbetta[6,7,8,9,10,11], Dimitri Van De Ville[1,2]

[1]Department of Radiology and Medical Informatics, University of Geneva, 1211 Geneva, Switzerland
[2]Medical Image Processing Laboratory, Center for Neuroprosthetics, Institute of Bioengineering, Ecole Polytechnique Fédérale de Lausanne (EPFL), 1202 Geneva, Switzerland
[3]Department of Physical Medicine and Rehabilitation, University of Pittsburgh, Pittsburgh, PA, USA
[4]Rehabilitation Neural Engineering Laboratories, University of Pittsburgh, Pittsburgh, PA, USA
[5]Bertarelli Foundation Chair in Translational Neuroengineering, Center for Neuroprosthetics, Institute of Bioengineering, Ecole Polytechnique Fédérale de Lausanne (EPFL), 1202 Geneva, Switzerland
[6]Department of Neurology, Washington University School of Medicine, St. Louis, MO, 63110, USA
[7]Department of Radiology, Washington University School of Medicine, St. Louis, MO, 63110, USA
[8]Department of Anatomy and Neurobiology, Washington University School of Medicine, St. Louis, MO, 63110, USA 7
[9]Department of Bioengineering, Washington University School of Medicine, St. Louis, MO, 63110, USA
[10]Department of Neuroscience and Padua Neuroscience Center, University of Padua, Padua, Italy
[11]Venetian Institute of Molecular Medicine (VIMM), Padua, Italy

[12]These authors contributed equally

*Dimitri Van de Ville.
Email: dimitri.vandeville@epfl.ch

Supplementary Material and Methods

Participants exclusion criteria

From the initial sample of 148 subjects, N = 24 patients and n = 2 healthy subjects were excluded from the analysis because of excessive motion (> 60% of volumes with a framewise displacement of more than 0.5 mm (1)) or because of a low number of significant innovation frames (< 131 significant innovation frames over a total of 808 volumes).

Behavioral domain scores

Dimensionality reduction was performed on the performance data as described in detail in (2, 3). First, tasks were categorized as attention, spatial memory, verbal memory, language, and motor. A PCA was run on the behavioral data of the session at 1-2 weeks post-lesion and the first component was used as a domain score for each category separately (see **SI** for a description of the components). The component scores for subsequent time points and for the age-matched controls were generated by normalizing the original data based on the sub-acute values and projecting them in the PCA space. Then, each of the components and time-points was z-scored based on the first measurement of the healthy control group, allowing comparisons across timepoints and behavioral domains. Patients with a score >/< 2 standard deviations were identified as “patients with/without severe acute deficits”. For each behavioral domain, we followed the same procedure as (3) and conducted an ANOVA across the three timepoints comparing patients with and without severe acute deficits. In attention, the first component described 24.7% of variance and was strongly related to measures of attentional field bias such as the total number of miss items in Mesulam cancellation test (r = 0.61), and the accuracy (r = 0.85) and reaction time (r = 0.72) in the Posner task. For the motor domain, the first two components (explained variance 40.0%

and 32.2% respectively) correlated with left and right motor function. In language the first component accounted for 77.3% of the variance and correlated with tasks of auditory comprehension, expression, and reading ($r > 0.81$). Finally, for spatial memory the first component (explained variance 61%) was correlated with measures of visuospatial memory such as immediate ($r = 0.87$) and delayed recall ($r = 0.90$) of visual information on the Brief Visuospatial Memory Test; whereas for verbal memory the first factor (explained variance 74.9%) correlates with measures from the Hopkins Verbal Learning Test such as delayed recall of words ($r = 0.96$).

Lesion masking

Individual T1 MRI images were registered to the MNI brain using FSL (FMRIB Software Library) FNIRT tool (4). Lesions were manually segmented on individual structural MRI images obtained 1–2 weeks post-lesion using the Analyze biomedical imaging software system (5). Special attention was given to distinguish lesion from CSF, hemorrhage from surrounding vasogenic edema, and to identify the degree of periventricular white matter damage present. In hemorrhagic strokes, edema was included in the lesion. The staff that was involved in segmenting or in reviewing the lesions (M.C. and Alexandre Carter) was blind to the individual behavioral data.

Total Activation and iCAPs

The Total Activation (TA) and iCAPs framework is based on the detection of significant changepoints in deconvolved fMRI time series. Matlab code for the application of the whole framework can be found at https://www.c4science.ch/source/iCAPs.
TA was applied for each subject and session to each run separately in order to obtain activity-inducing time courses. For each subject, activity-inducing time courses were contacted over all runs and activation change-points were computed as the temporal derivative of these activity-inducing signals. In order to select significant innovations frames (i.e., frames with significant transitioning activities - transients), a two-step thresholding procedure was employed with temporal and spatial thresholds selected based on previous work (6–8): i) temporal thresholding - for each voxel, a surrogate distribution was obtained by applying TA on phase randomized data and a 1% confidence interval was used to select significant voxels; ii) spatial thresholding - only the innovation frames with at least 5% of active voxels were considered to be significant. Transients were then normalized to Montreal Neurological Institute (MNI) and concatenated across all subjects (i.e., patients and healthy subjects) and sessions, and fed into a temporal k-means clustering to obtain large-scale resting-state networks, the iCAPs. The optimum number of clusters was determined by evidence accumulation (9, 10) (see **Figures S3a**). Briefly, the k-means clustering was done for K values ranging from 10 to 24, in order to obtain a co-association matrix summarizing how often two frames were clustered together. A second phase of clustering was performed using this co-association matrix and, this time, hierarchical clustering with two different linkage functions (average and weighted). We then computed the percentage of agreement between these two linkage functions, as well as with the k-means solution. The number of iCAPs was chosen as the number that showed the highest percentage of agreement, thus resulting in the extraction 16 iCAPs.

Partial Least Squares Correlation

Partial least squares correlation (PLSC) has been previously successfully employed to characterize covarying patterns of structural and functional connectivity in healthy individuals (11), and it is nowadays considered a clinically relevant method (7, 12–15). It seeks to define linear combinations of two data matrices (**X**, i.e., the brain networks properties – iCAP durations, and **Y,** i.e., the behavioral or anatomical variables) that maximally explain the covariance between the two matrices. The first step in PLSC is the computation of the correlation matrix between **X** and **Y** (**R = X'Y**). In our approach, **X** and **Y** were z-scored across subjects before correlation. Then **R** is decomposed in *N* latent variables, or "correlation components" (where *N* is the minimum number between the number of included behavioral/anatomical variables and the number of iCAPs), using singular value composition **R=USV'** with **U'U=V'V=I**. Each correlation component has a singular value (on the diagonal of **S**) that specifies the explained correlation, as well as *Nx* iCAP durations saliences or "duration weights" (rows of **V'**) and *Ny* behavioral/anatomical saliences or

"behavioral/anatomical weights" (columns of **U**). The saliences (which lie between -1 and 1) indicate how strongly each variable contributes to the multivariate behavioral-brain/anatomical-brain correlation in a certain correlation component. We can then compute the so called "brain scores" by projecting every individual's iCAP durations onto the respective brain weights with **Lx=XV**. We used permutation testing with 1000 permutations to evaluate if any of the correlation components was significant and bootstrapping with 500 bootstrap samples with replacement to evaluate the stability of the behavior/anatomical and brain weights. Brain and behavioral saliences were recalculated for every bootstrap sample, resulting in a typical bootstrap distributing of the salience values. Saliences were considered significant if lower/higher than lower/upper bound of 95% confidence interval of bootstrapping distributions.

Group PLSC analysis, as the one used for the correlation between iCAP durations and behavioral scores, entails that a correlation matrix is computed per group (in this case healthy controls $\mathbf{R_{HC}}$, patients with less severe acute deficits $\mathbf{R_{ND}}$, and patients with severe acute deficits $\mathbf{R_{D}}$). The common correlation matrix R is then computed by concatenating $\mathbf{R_{HC}}$, $\mathbf{R_{ND}}$ and $\mathbf{R_{D}}$ resulting in $3Ny$ behavior saliences.

Data availability

As the clinical effectiveness of all these methods is critically dependent on the availability of publicly released tools (16), the full set of neuroimaging data (along with behavioral data) are available at http://cnda.wustl.edu /app/template/Login and the scripts for the iCAP framework and PLSC analysis are openly accessible (https://c4science.ch/source/iCAPs/ and https://github.com/danizoeller/myPLS, respectively). Other specific data and scripts are available upon request to the authors.

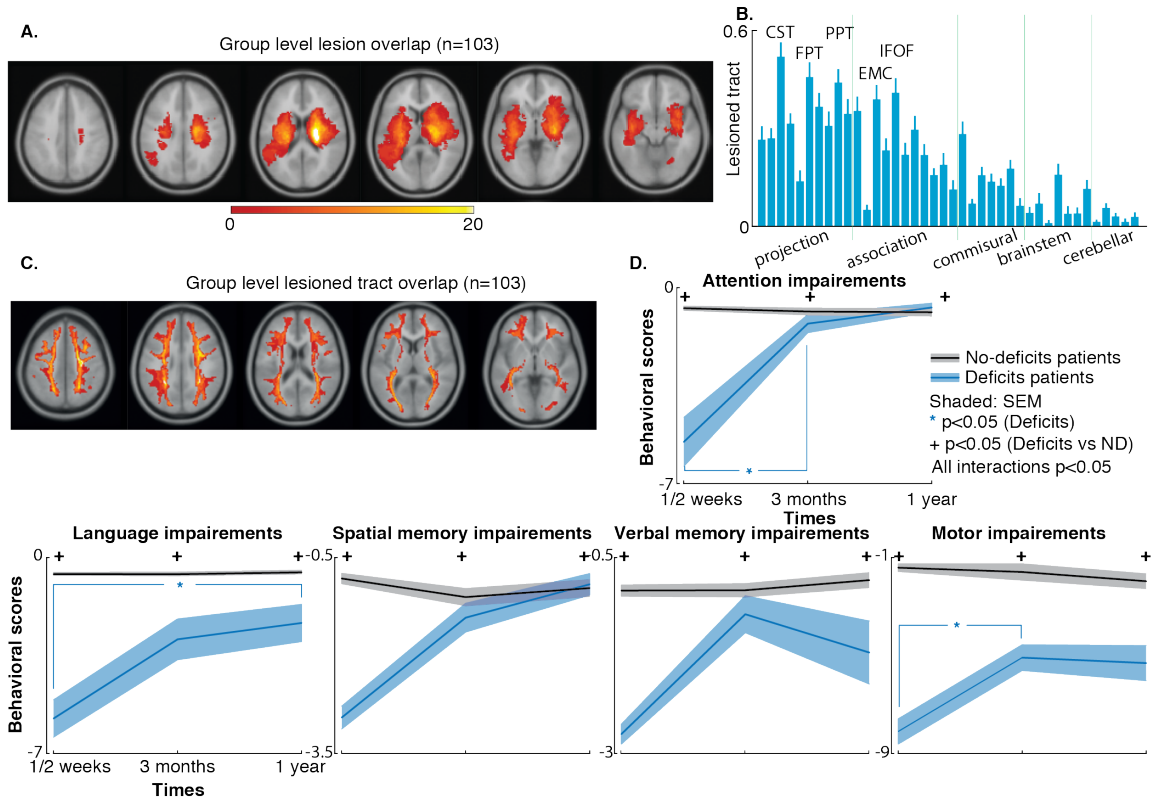

Fig. S1. Patient population | A. Topography of stroke. Binary lesion masks of all 103 stroke patients included in the analysis were summed and overlaid in Montreal Neurological Institute coordinates. **B.** Mean ± SEM over subjects of the portion of streamlines disconnected for each tract. Tracts were grouped in projection pathways, association pathways, commissural pathways, brain- stem pathways, and cerebellar pathways following (17). **C.** Streamlines disconnected overlay map in Montreal Neurological Institute coordinates for the 103 stroke patients included in the analysis. **D.** Time course of recovery for each domain separately (e.g., attention (n=81 subjects), language (n=96), spatial memory (n=76), verbal memory (n=76), and motor (n=89)). We reported behavioral factor scores over the three time points for patients that have severe deficits (blue lines) and did not (black lines) have severe deficit 1-2 weeks post stroke (mean ± SEM over subjects). Interactions between the two groups over time are significant for each domain (as indicated by + symbols). * represents significant differences (corrected for multiple comparisons) within timepoints for patients that did have severe acute deficits.

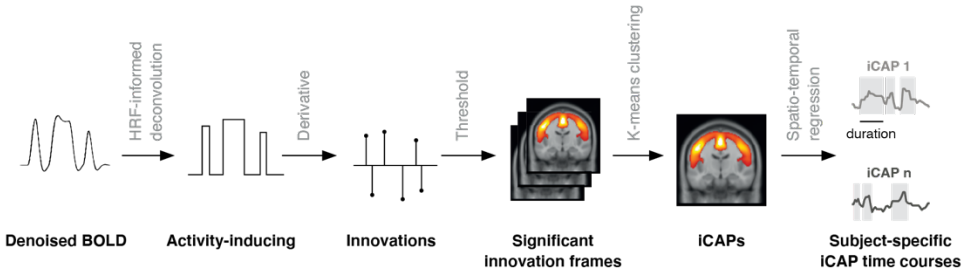

Fig. S2. Dynamic functional connectivity framework | Functional images from individual subjects are denoised to circumvent the effect of various sources of noise. The hemodynamic blur is subsequently removed using hemodynamic-informed deconvolution, which reveals the activity-inducing signals. The innovation frames are then obtained by temporal derivation. A two-step thresholding (temporal and spatial) is applied to select significant innovation frames (i.e., transients), which undergo temporal clustering over subjects to obtain stable iCAPs. The latter are fitted back to the individual activity inducing signals to recover temporal profiles of the iCAPs for further time-resolved analysis. For each participant, session, and iCAP, we then computed the average duration over the total acquisition length.

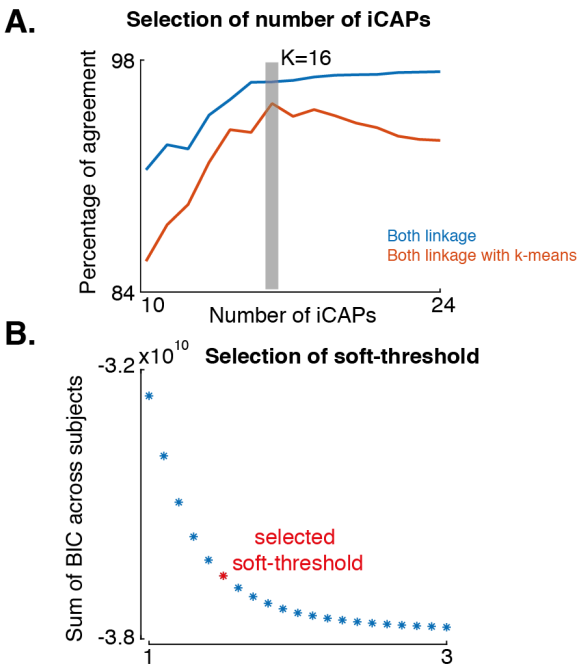

Fig. S3. Parameters selections for the dynamic functional connectivity framework | A. Percentage of agreement for linkage (blue) and linkage with k-means (orange) for number of iCAPs from 10 to 24. The number of iCAPs was chosen as the number at which both methods had the highest percentage (i.e., k=16 iCAPs). **B.** Evaluation of soft assignment factors ξ from 1 (hard cluster assignment) to 3 (all iCAPs allowed to change at timepoints of significant transients). The red dot indicates the selected soft-threshold (i.e.,$\xi = \mathbf{1.5}$) (see (18) for details).

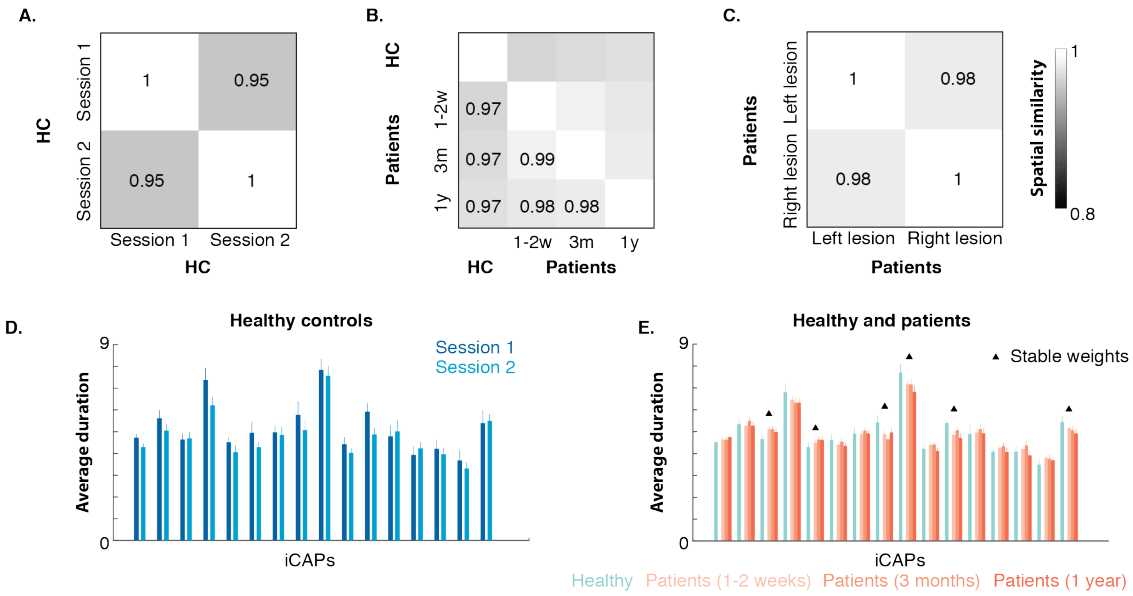

Fig. S4. Stability of spatial patterns and average duration | A. Cosine similarity between iCAPs spatial patterns of healthy control subject's session 1 and session 2 averaged over the 16 iCAPs. **B.** Cosine similarity between iCAPs spatial patterns for healthy control subjects and stroke patients at 1-2 weeks, 3 months, and one-year post-lesion averaged over the 16 iCAPs. **C.** Cosine similarity between iCAPs spatial patterns of patients with lesion in the left hemisphere and patients with lesion in the right hemisphere. **D.** iCAPs average duration for healthy control subject's session 1 (dark blue) and session 2 (light blue) (mean ± SEM over subjects). **E.** iCAPs average duration for healthy control subjects averaged over session 1 and 2 (cyan), patients at 1-2 weeks (light orange), 3 months (orange), and one-year post-lesion (dark orange) (mean ± SEM over subjects). Triangle indicates iCAPs that have stable weights over folds of the LDA classifier.

Table S1. Patients demographics | Age, Sex, Dominant Hand, Education, Lesion Side, Lesion Type, number of participants included for the 5 different behavioral domains (Attention, Spatial Memory, Verbal Memory, Motor, and Language), and time between lesion onset and scans at different time points T_0 (1/2 weeks), T_1 (3 months), and T_2 (1-year post-lesion). SD: Standard Deviation; M: Male; F: Female; R: Right; L: Left; I: Ischemic; H: Hemorrhagic; O: other stroke etiologies (e.g. hemorrhagic conversion, vertebral artery dissection, etc.); Att: Attention; Mem: Memory; Mot: Motor; Lan: Language.

Group	Age (Mean/SD)	Sex	Hand	Education (Mean/SD)	Lesion Side	Lesion Type	Att.	Spatial Mem.	Verbal Mem.	Mot.	Lang.	Time (Mean/SD)
Patients (N=103)	53.5/10.2	59M/ 44F	95R/8L	13/2.5	47R/56L	80%I 15%H 5% O	81	76	76	89	96	T_0: 13.4d/4.8d T_1: 112.5d/8.4d T_2: 395.5d/55.1d
Controls (N=19)	52.7/12.8	7M/ 12F	17R/2L	13.8/2.4	N/A	N/A	19	19	19	19	19	N/A

Table S2. iCAPs | iCAP functional networks of Greicius atlas (19), iCAP regions in the automated anatomical labeling (AAL) atlas (20) and 34 regions corresponding to portions of the cerebellum, thalamus, and basal ganglia taken from the automatic anatomical labeling (AAL) atlas. Percentiles indicate the fraction of voxels of a functional network or region that have a z-score > 1.9. A network/region is listed if more than 20% of the network/region is included in the iCAP.

iCAP	Greicius network (%)	AAL Lobe	AAL Region (%)	z-score	N vox
1	Primary visual (99%)	Occipital	Cuneus_L (67%)	3.19	298
	Precuneus (63%)	Occipital	Cuneus_R (65%)	3.16	283
	DMN (33%)	Occipital	Calcarine_L (53%)	3.31	343
		Occipital	Calcarine_R (63%)	3.26	340
		Occipital	Lingual_L (32%)	2.79	211
		Occipital	Lingual_R (28%)	2.80	188
		Occipital	Occipital_Sup_L (23%)	2.53	91
		Parietal	Precuneus_L (30%)	2.73	326
		Parietal	Precuneus_R (35%)	2.83	324
2	High visual (46%)	Occipital	Occipital_Inf_L (30%)	2.46	80
	Cerebellum(26%)	Occipital	Occipital_Inf_R (25%)	2.51	77
		Occipital	Fusiform_L (23%)	2.74	153
		Occipital	Lingual_R (21%)	2.72	142
		Cereb	Cerebellum_Crus1_L (50%)	2.58	380
		Cereb	Cerebellum_Crus1_R (41%)	2.41	327
		Cereb	Cerebellum_6_L (79%)	2.56	407
		Cereb	Cerebellum_6_R (65%)	2.44	351
		Cereb	Cerebellum_Crus2_L (30%)	2.35	172
		Vermis	Vermis_6 (85%)	2.39	89
		Vermis	Vermis_7 (95%)	2.70	56
		Vermis	Vermis_8 (70%)	2.33	47
3	Sensorimotor (37%)	Parietal	Postcentral_L (44%)	2.89	512
	Auditory (27%)	Parietal	Postcentral_R (26%)	2.60	297
	Visuospatial (28%)	Parietal	Paracentral_Lobule_L (36%)	2.76	154
		Parietal	Paracentral_Lobule_R (32%)	2.61	72
		Limbic	Cingulum_Mid_L (38%)	2.86	236
		Limbic	Cingulum_Mid_R (30%)	2.87	180
		Frontal	Supp_Motor_Area_L (33%)	3.06	214
		Frontal	Supp_Motor_Area_R (31%)	2.98	207
		Frontal	Precentral_L (27%)	2.67	277
		Frontal	Precentral_R (21%)	2.65	202
4	DMN (41%)	Frontal	Frontal_Sup_Medial_L (45%)	2.97	383
	Precuneus (22%)	Frontal	Frontal_Sup_Medial_R (39%)	2.80	253
	ECN (33%)	Frontal	Frontal_Sup_L (24%)	2.80	254
	Anterior Salience (45%)	Frontal	Frontal_Mid_L (29%)	2.72	419
		Limbic	Cingulum_Ant_L (27%)	2.69	117
		Limbic	Cingulum_Ant_R (36%)	2.72	141
		Parietal	Angular_L (27%)	2.51	92
5	Auditory (93%)	Temporal	Heschl_L (94%)	3.50	68
	Language (22%)	Temporal	Heschl_R (92%)	3.75	67
		Temporal	Temporal_Sup_L (57%)	3.05	386
		Temporal	Temporal_Sup_R (54%)	3.03	521
		Central	Rolandic_Oper_L (67%)	3.16	203
		Central	Rolandic_Oper_R (70%)	3.16	281
		Limbic	Insula_L (68%)	3.15	385
		Limbic	Insula_R (70%)	3.27	375
		Frontal	Frontal_Inf_Oper_R (21%)	2.76	90
6	Primary visual (99%)	Occipital	Calcarine_L (52%)	2.85	336
	High visual (64%)	Occipital	Calcarine_R (68%)	2.92	368
		Occipital	Lingual_L (65%)	2.94	435

		Occipital	Lingual_R (68%)	3.00	463
		Occipital	Occipital_Mid_L (22%)	2.59	211
		Occipital	Occipital_Mid_R (22%)	2.72	133
		Occipital	Occipital_Inf_L (30%)	2.64	81
		Occipital	Occipital_Inf_R (21%)	2.67	66
		Occipital	Fusiform_R (25%)	2.76	188
		Cereb	Cerebellum_4_5_L (30%)	2.30	106
		Cereb	Cerebellum_4_5_R (31%)	2.30	76
		Cereb	Cerebellum_6_L (59%)	2.51	306
		Cereb	Cerebellum_6_R (57%)	2.43	304
		Vermis	Vermis_4_5 (63%)	2.41	116
		Vermis	Vermis_6 (96%)	2.64	101
		Vermis	Vermis_7 (63%)	2.07	37
7	Cerebellum (22%)	Limbic	Hippocampus_L (52%)	2.20	143
	Amygdala (23%)	Limbic	Hippocampus_R (65%)	2.29	188
		Limbic	ParaHippocampal_L (27%)	2.46	77
		Limbic	ParaHippocampal_R (30%)	2.62	94
		Occipital	Lingual_L (26%)	2.25	172
		Occipital	Lingual_R (29%)	2.29	198
		Occipital	Fusiform_L (27%)	2.30	184
		Occipital	Fusiform_R (43%)	2.37	328
		Cereb	Cerebellum_3_L (35%)	2.23	14
		Cereb	Cerebellum_3_R (43%)	2.39	27
		Cereb	Cerebellum_4_5_L (71%)	2.62	256
		Cereb	Cerebellum_4_5_R (86%)	2.71	208
		Cereb	Cerebellum_6_L (71%)	2.33	367
		Cereb	Cerebellum_6_R (72%)	2.43	389
		Vermis	Vermis_3 (40%)	2.25	27
		Vermis	Vermis_4_5 (75%)	2.57	138
		Vermis	Vermis_6 (88%)	2.47	92
		Vermis	Vermis_7 (51%)	2.14	30
		Vermis	Vermis_8 (37%)	2.04	25
		Vermis	Vermis_9 (40%)	2.00	23
8	Sensorimotor (33%)	Frontal	Precentral_L (30%)	2.83	308
	Ventral DMN (26%)	Frontal	Precentral_R (37%)	3.00	370
	Anterior Salience (24%)	Frontal	Supp_Motor_Area_L (68%)	2.89	445
	Visuospatial (27%)	Frontal	Supp_Motor_Area_R (76%)	3.00	504
		Frontal	Frontal_Sup_R (21%)	2.95	245
		Parietal	Postcentral_L (26%)	2.74	299
		Parietal	Postcentral_R (37%)	3.12	420
		Parietal	Parietal_Sup_L (25%)	2.55	160
		Parietal	Parietal_Sup_R (32%)	2.72	208
		Parietal	Precuneus_L (30%)	2.72	318
		Parietal	Precuneus_R (23%)	2.71	214
		Parietal	Paracentral_Lobule_L (68%)	3.26	287
		Parietal	Paracentral_Lobule_R (70%)	3.32	125
		Parietal	Parietal_Inf_R (30%)	2.51	419
		Limbic	Cingulum_Mid_L (29%)	2.42	182
		Limbic	Cingulum_Mid_R (24%)	2.46	148
9	Amygdala (78%)	Frontal	Frontal_Sup_Orb_L (26%)	2.24	105
		Frontal	Frontal_Sup_Orb_R (42%)	2.25	132
		Frontal	Frontal_Inf_Orb_L (41%)	2.31	205
		Frontal	Frontal_Inf_Orb_R (31%)	2.32	154
		Frontal	Olfactory_L (51%)	2.21	44
		Frontal	Olfactory_R (53%)	2.24	43
		Frontal	Rectus_L (88%)	2.34	230
		Frontal	Rectus_R (91%)	2.35	199
		Frontal	Frontal_Sup_Orb_Medial_L (21%)	2.06	47
		Limbic	Hippocampus_L (42%)	2.92	116

		Limbic	Hippocampus_R (46%)	2.94	132
		Limbic	ParaHippocampal_L (35%)	2.80	99
		Limbic	ParaHippocampal_R (40%)	2.83	127
		Limbic	Amygdala_L (82%)	2.56	51
		Limbic	Amygdala_R (77%)	2.52	54
		Temporal	Temporal_Pole_Sup_L (38%)	2.38	145
		Temporal	Temporal_Pole_Sup_R (31%)	2.32	123
		Temporal	Temporal_Pole_Mid_L (44%)	2.73	97
		Temporal	Temporal_Pole_Mid_R (39%)	2.57	136
		Temporal	Temporal_Inf_L (50%)	3.06	471
		Temporal	Temporal_Inf_R (40%)	2.98	433
		Temporal	Temporal_Mid_L (20%)	2.74	292
		Occipital	Fusiform_L (26%)	3.11	181
		Occipital	Fusiform_R (45%)	3.13	194
10	Precuneus (85%)	Parietal	Parietal_Sup_L (50%)	3.04	315
	DMN (41%)	Parietal	Parietal_Sup_R (40%)	3.05	257
	Visuospatial (38%)	Parietal	Parietal_Inf_L (43%)	2.62	299
		Parietal	Parietal_Inf_R (57%)	2.92	240
		Parietal	Angular_L (31%)	2.35	105
		Parietal	Angular_R (49%)	2.91	241
		Parietal	Precuneus_L (65%)	3.11	700
		Parietal	Precuneus_R (67%)	3.22	629
		Parietal	Paracentral_Lobule_R (21%)	2.28	47
		Occipital	Cuneus_L (46%)	2.51	206
		Occipital	Cuneus_R (55%)	2.70	239
		Occipital	Occipital_Sup_L (39%)	2.74	156
		Occipital	Occipital_Sup_R (47%)	3.14	203
		Occipital	Occipital_Mid_R (25%)	2.76	149
		Limbic	Cingulum_Mid_L (25%)	2.65	156
		Limbic	Cingulum_Mid_R (22%)	2.61	135
		Limbic	Cingulum_Post_L (36%)	2.38	49
11	Primary visual (97%)	Occipital	Calcarine_L (65%)	3.20	423
	High visual (42%)	Occipital	Calcarine_R (82%)	3.35	446
	Precuneus (54%)	Occipital	Cuneus_L (85%)	3.60	382
		Occipital	Cuneus_R (89%)	3.71	387
		Occipital	Lingual_L (41%)	2.56	270
		Occipital	Lingual_R (43%)	2.50	294
		Occipital	Occipital_Sup_L (74%)	3.29	292
		Occipital	Occipital_Sup_R (73%)	3.29	313
		Occipital	Occipital_Mid_L (53%)	2.74	511
		Occipital	Occipital_Mid_R (61%)	2.97	361
		Parietal	Precuneus_R (23%)	2.51	214
12	Dorsal DMN (41%)	Frontal	Frontal_Sup_Orb_L (49%)	2.77	143
		Frontal	Frontal_Sup_Orb_R (47%)	2.72	146
		Frontal	Frontal_Mid_Orb_L (51%)	2.92	139
		Frontal	Frontal_Mid_Orb_R (43%)	2.90	127
		Frontal	Frontal_Inf_Tri_L (27%)	2.54	193
		Frontal	Frontal_Inf_Tri_R (21%)	2.47	133
		Frontal	Frontal_Inf_Orb_L (43%)	2.66	215
		Frontal	Frontal_Inf_Orb_R (38%)	2.75	193
		Frontal	Olfactory_L (32%)	2.60	28
		Frontal	Olfactory_R (39%)	2.45	32
		Frontal	Frontal_Sup_Medial_L (24%)	3.03	200
		Frontal	Frontal_Sup_Medial_R (22%)	3.09	144
		Frontal	Frontal_Sup_Orb_Medial_L (77%)	3.55	174
		Frontal	Frontal_Sup_Orb_Medial_R (81%)	2.64	212
		Frontal	Rectus_L (67%)	2.64	174
		Frontal	Rectus_R (63%)	2.63	128
		Limbic	Insula_L (21%)	2.38	121

		Limbic	Insula_R (24%)	2.37	131
		Limbic	Cingulum_Ant_L (64%)	3.72	271
		Limbic	Cingulum_Ant_R (61%)	3.26	241
		Subcortical	Caudate_L (48%)	2.93	134
		Subcortical	Caudate_R (50%)	2.88	144
		Subcortical	Putamen_L (26%)	2.51	81
		Subcortical	Putamen_R (27%)	2.55	87
13	Cerebellum (51%)	Occipital	Fusiform_R (27%)	2.36	204
		Cereb	Cerebellum_Crus1_L (52%)	3.07	391
		Cereb	Cerebellum_Crus1_R (55%)	3.23	434
		Cereb	Cerebellum_Crus2_L (43%)	2.87	247
		Cereb	Cerebellum_Crus2_R (33%)	3.07	202
		Cereb	Cerebellum_3_L (28%)	2.09	11
		Cereb	Cerebellum_3_R (32%)	2.43	20
		Cereb	Cerebellum_4_5_L (60%)	2.71	216
		Cereb	Cerebellum_4_5_R (72%)	2.83	175
		Cereb	Cerebellum_6_L (91%)	3.22	470
		Cereb	Cerebellum_6_R (88%)	3.53	473
		Cereb	Cerebellum_7b_L (36%)	2.90	64
		Cereb	Cerebellum_7b_R (24%)	2.70	39
		Cereb	Cerebellum_8_L (36%)	2.83	201
		Cereb	Cerebellum_8_R (33%)	3.01	223
		Cereb	Cerebellum_9_L (51%)	2.77	129
		Cereb	Cerebellum_9_R (52%)	2.85	127
		Vermis	Vermis_4_5 (58%)	2.78	106
		Vermis	Vermis_6 (97%)	3.52	102
		Vermis	Vermis_7 (100%)	3.98	59
		Vermis	Vermis_8 (100%)	3.74	67
		Vermis	Vermis_9 (98%)	3.68	56
		Vermis	Vermis_10 (63%)	2.66	19
14	Anterior salience (52%)	Frontal	Frontal_Sup_L (44%)	3.33	471
		Frontal	Frontal_Sup_R (45%)	3.19	521
		Frontal	Frontal_Mid_L (31%)	2.87	452
		Frontal	Frontal_Mid_R (33%)	2.84	500
		Frontal	Supp_Motor_Area_L (71%)	3.21	468
		Frontal	Supp_Motor_Area_R (59%)	3.28	394
		Frontal	Frontal_Sup_Medial_L (39%)	3.57	331
		Frontal	Frontal_Sup_Medial_R (40%)	3.67	259
		Limbic	Cingulum_Mid_L (24%)	2.58	150
		Limbic	Cingulum_Mid_R (33%)	2.84	202
15	Dorsal DMN (44%)	Frontal	Frontal_Sup_L (36%)	3.43	389
	Anterior salience (42%)	Frontal	Frontal_Sup_R (30%)	3.33	343
		Frontal	Frontal_Mid_L (30%)	3.08	436
		Frontal	Frontal_Mid_R (30%)	2.80	460
		Frontal	Frontal_Inf_Tri_L (22%)	2.33	163
		Frontal	Frontal_Sup_Medial_L (62%)	3.70	527
		Frontal	Frontal_Sup_Medial_R (60%)	3.40	383
		Limbic	Cingulum_Ant_L (79%)	3.57	338
		Limbic	Cingulum_Ant_R (87%)	3.76	346
16	Cerebellum (44%)	Cereb	Cerebellum_Crus1_L (59%)	2.47	445
	ECN (27%)	Cereb	Cerebellum_Crus1_R (53%)	2.59	425
		Cereb	Cerebellum_Crus2_L (78%)	3.63	452
		Cereb	Cerebellum_Crus2_R (60%)	3.63	372
		Cereb	Cerebellum_7b_L (71%)	3.80	127
		Cereb	Cerebellum_7b_R (61%)	3.87	98
		Cereb	Cerebellum_8_L (64%)	3.23	353
		Cereb	Cerebellum_8_R (60%)	3.33	407
		Cereb	Cerebellum_9_L (56%)	2.83	142
		Cereb	Cerebellum_9_R (57%)	2.87	138

		Vermis	Vermis_7 (71%)	2.63	42
		Vermis	Vermis_8 (72%)	3.60	48
		Vermis	Vermis_9 (65%)	2.53	37

SI References

1. J. D. Power, K. A. Barnes, A. Z. Snyder, B. L. Schlaggar, S. E. Petersen, Spurious but systematic correlations in functional connectivity MRI networks arise from subject motion. *Neuroimage* **59**, 2142–2154 (2012).

2. M. Corbetta, *et al.*, Common behavioral clusters and subcortical anatomy in stroke. *Neuron* **85**, 927–941 (2015).

3. L. Ramsey, *et al.*, Behavioural clusters and predictors of performance during recovery from stroke. *Nature human behaviour* **1**, 1–10 (2017).

4. J. L. Andersson, M. Jenkinson, S. Smith, Non-linear optimisation. FMRIB technical report TR07JA1. *Practice* (2007).

5. R. A. Robb, D. P. Hanson, A software system for interactive and quantitative visualization of multidimensional biomedical images. *Australasian Physical & Engineering Sciences in Medicine* **14**, 9–30 (1991).

6. F. I. Karahanoğlu, D. Van De Ville, Transient brain activity disentangles fMRI resting-state dynamics in terms of spatially and temporally overlapping networks. *Nature communications* **6**, 1–10 (2015).

7. D. Zöller, *et al.*, Large-scale brain network dynamics provide a measure of psychosis and anxiety in 22q11. 2 deletion syndrome. *Biological Psychiatry: Cognitive Neuroscience and Neuroimaging* **4**, 881–892 (2019).

8. A. Tarun, *et al.*, NREM sleep stages specifically alter dynamical integration of large-scale brain networks. *iScience*, 101923 (2020).

9. A. L. Fred, A. K. Jain, Data clustering using evidence accumulation in (IEEE, 2002), pp. 276–280.

10. A. L. Fred, A. K. Jain, Combining multiple clusterings using evidence accumulation. *IEEE transactions on pattern analysis and machine intelligence* **27**, 835–850 (2005).

11. B. Mišić, *et al.*, Network-level structure-function relationships in human neocortex. *Cerebral Cortex* **26**, 3285–3296 (2016).

12. J. C. Griffis, N. V. Metcalf, M. Corbetta, G. L. Shulman, Structural disconnections explain brain network dysfunction after stroke. *Cell reports* **28**, 2527–2540 (2019).

13. D. Zöller, *et al.*, Disentangling resting-state BOLD variability and PCC functional connectivity in 22q11. 2 deletion syndrome. *Neuroimage* **149**, 85–97 (2017).

14. D. Zöller, *et al.*, Psychotic symptoms influence the development of anterior cingulate BOLD variability in 22q11. 2 deletion syndrome. *Schizophrenia research* **193**, 319–328 (2018).

15. A. Krishnan, L. J. Williams, A. R. McIntosh, H. Abdi, Partial Least Squares (PLS) methods for neuroimaging: a tutorial and review. *Neuroimage* **56**, 455–475 (2011).

16. T. A. Bolton, E. Morgenroth, M. G. Preti, D. Van De Ville, Tapping into multi-faceted human behavior and psychopathology using fMRI brain dynamics. *Trends in Neurosciences* (2020).

17. F. C. Yeh, *et al.*, Population-averaged atlas of the macroscale human structural connectome and its network topology. *NeuroImage* **178**, 57–68 (2018).

18. D. M. Zöller, *et al.*, Robust recovery of temporal overlap between network activity using transient-informed spatio-temporal regression. *IEEE Transactions on Medical Imaging* **38**, 291–302 (2018).

19. W. R. Shirer, S. Ryali, E. Rykhlevskaia, V. Menon, M. D. Greicius, Decoding subject-driven cognitive states with whole-brain connectivity patterns. *Cerebral cortex* **22**, 158–165 (2012).

20. N. Tzourio-Mazoyer, *et al.*, Automated anatomical labeling of activations in SPM using a macroscopic anatomical parcellation of the MNI MRI single-subject brain. *Neuroimage* **15**, 273–289 (2002).